http://dx.doi.org/10.5012/bkcs.2013.34.1.68

Enhanced Raman Spectrum of Juglone on Ag Surface: Is It a Simile to That of Lawsone?

Byeong-Seo Cheong and Han-Gook Cho*

*Department of Chemistry, University of Incheon, Incheon 406-772, Korea. *E-mail: hgc@incheon.ac.kr*
Received September 17, 2012, Accepted October 9, 2012

The surface enhanced Raman spectrum of juglone, a traditional natural dye, has been observed by a custom-built micro-Raman setup. The spectral features of juglone significantly differ from those of lawsone, a structural isomer of juglone; only small red shifts of the double bond stretching bands are observed, and strong SERS bands are observed in the lower frequency regions as well. The DFT computations reveal that juglone coordinated to an Ag^+ adatom with H^+ release best correlates with the observed vibrational characteristics in the SERS spectrum among the plausible configurations of juglone coordinated to an adatom on the Ag surface, in line with the previously studied lawsone case. The differences in the SERS spectra of juglone and lawsone are attributed to the different locations of the hydroxyl group in the two isomers.

Key Words : Juglone, Raman, Surface enhancement, Ag colloid, DFT

Introduction

Juglone, one of the best known natural dyes, is called by various other names such as C. I. Natural Brown 7, C. I. 75500, and Nucin. It has also been used as an herbicide due to its toxicity. Tracing the use of organic colorants is essential for dating, restoring, and conserving paintings and artworks,[1] due to their distinctive roles for communications, textiles, and arts in human history.[2] The concentrations of organic colorants in artistic and archaeological objects are, however, normally very low. Thus, the plasmonic enhancement on coinage metal surface, particularly in conjunction with microscopy, opens a new way for analysis of these trace components.[3]

Juglone (5-hydroxy-1,4-naphthalenedione), a combination of phenol and quinone rings (Figure 1), is an isomer of lawsone (2-hydroxy-1,4-naphthoquinone), another well-known natural dye.[2] The only difference between these two dyes is the location of the hydroxyl group; the –OH group is part of the phenol ring in juglone, whereas it is bonded to the quinone ring in lawsone. In the surface-enhanced Raman scattering (SERS) spectrum of lawsone, which has recently been investigated, the strong bands in the double-bond stretching region (1800-1500 cm^{-1}) show large red shifts (~50 cm^{-1}) from those in the infrared and powder Raman spectra.[4] The in-plane stretching bands enhanced by the surface plasmon also indicate that the molecular plane is perpendicular to the Ag plane. DFT computations show that lawsone (with H^+ release) coordinated to the Ag^+ adatom best reproduces the observed SERS spectrum.[4]

In this study the SERS spectrum of juglone[5] is investigated with a recently built micro-Raman setup. The difference in location of the hydroxyl group leads to considerable variations in the spectra, the small frequency shifts in the double-bond stretching region and the strong bands in the lower frequency regions. DFT computations are performed to provide support for the assignment of the observed frequencies and the plausible configuration of juglone on the Ag surface.

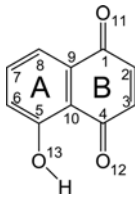

Figure 1. Atom numbering of juglone used in this study. Notice that the phenol and quinone rings are designated to rings A and B.

Experimental and Computational Methods

The SERS spectra were measured with a micro-Raman spectrometer, which is custom-built around a commercial, inverted microscope (Olympus, IX71). The micro-Raman spectrometer has been described in detail elsewhere.[4] Briefly, the laser beam of a He-Ne laser is filtered by a narrow bandpass filter and its power adjusted to ~8 mW using a neutral density filter. It is directed into a 40× objective by a dichroic beamsplitter. The backscattered Raman signal was collected using the same objective lens, and directed into a spectrograph (Acton Research, Spectra Pro 2500) equipped with a TE-cooled, back-illuminated CCD detector (Princeton Instrument, PIXIS:100B). The Rayleigh scattered light was removed using an edge filter. The spectral resolution was estimated to be 4 cm^{-1} with the 300 grooves/mm grating based on the extent of the isotopic splitting in the $CHCl_3$ spectrum.[6]

The IR spectra were recorded at 1.0 cm^{-1} resolution with a Bruker Vertex 80V spectrometer, and the solid dye sample was dispersed in KBr. The solid powder FT-Raman spectra were obtained at 4.0 cm^{-1} resolution with a Bruker RFS100/

S spectrometer using the 1064 nm Nd:YAG laser (~50 mW) for excitation. UV/visible absorption spectra were recorded with quartz cells of 1 cm path length.

Silver nitrate (99.85%, Acros) and sodium citrate dihydrate (99.0%, Sigma-Aldrich) were used with no further purification. Doubly distilled, deionized water was used for all aqueous solution preparation, and all glassware was cleaned by aqua regia solution, and rinsed completely with distilled water. The Ag colloids were prepared by the Lee and Meisel procedure,[7a] reduction of silver nitrate with sodium citrate. The silver particle was observed spherical in shape with scanning electron microscope (SEM, Hitachi S-4300SE) and its diameter was estimated to be 10-80 nm.[7b]

The stock solution of juglone (Aldrich) was prepared in methanol at a concentration of 1 mM. The SERS sample were prepared as in the previous study,[4] and the typical concentrations of juglone and KNO_3 in the sample solution were 20 μM and 40 mM. The activation *via* KNO_3 solution or other anions is necessary to enhance the SERS signal. SERS measurements were made directly from a drop of the solution deposited on a microscope coverglass.

To provide support for the assignment of new experimental frequencies and to correlate with related works,[4,8] density functional theory (DFT) calculations were performed using the Gaussian 09 program system.[9] The B3LYP density functional,[10] the 6-311++G(3df,3pd) basis sets for H, C, and O,[11] and SDD core potential and basis sets for Ag[12] were employed to obtain vibrational frequencies for juglone free and coordinated to the adatom on Ag surface. Geometries were fully relaxed during optimization, and the optimized geometry was confirmed by vibrational analysis. The BPW91[13] functional was also employed to complement the B3LYP results.

The vibrational frequencies were calculated analytically, and the zero-point energy was included in the calculation of binding and reaction energies. DFT calculated harmonic frequencies provide useful predictions for vibrational spectra of new chemical species. However, they are usually slightly higher than observed frequencies,[14] and hence, a scale factor of 0.97 was used for the B3LYP harmonic frequencies to compare with the observed values, whereas no scale factor was employed for the BPW91 frequencies, which are normally smaller than the B3LYP values.

Results and Discussion

The enhanced Raman spectrum of juglone on the Ag surface with our micro-Raman spectrometer was illustrated with the infrared and powder FT-Raman spectra (Figures 2-4). The observed vibrational characteristics of juglone are compared with the DFT computation results in Table 1 and Figures 2 and 3. The simulated Raman spectra based on the DFT results for the plausible juglone configurations (Figure 6) are also shown in Figure 7.

Juglone Spectra. The infrared and FT-Raman spectra of juglone in powder form are shown with the simulated Raman spectrum deduced from DFT calculation in Figure 2. Due to its high surface reflectance of solid juglone, the FT-Raman spectrum is noisy and the band intensities are low.[5] It is, however, still noticeable that the infrared and FT-Raman spectra differ substantially in their band intensities, but most of their frequencies correspond one another between the two spectra. The measured frequencies from the spectra are listed in Tables 1. The strong bands in the characteristic double-bond stretching region (1800-1500 cm^{-1}) indicate that the double-bond stretching motions of the natural dye yield significant changes in the polarizability as well as in the dipole moment.

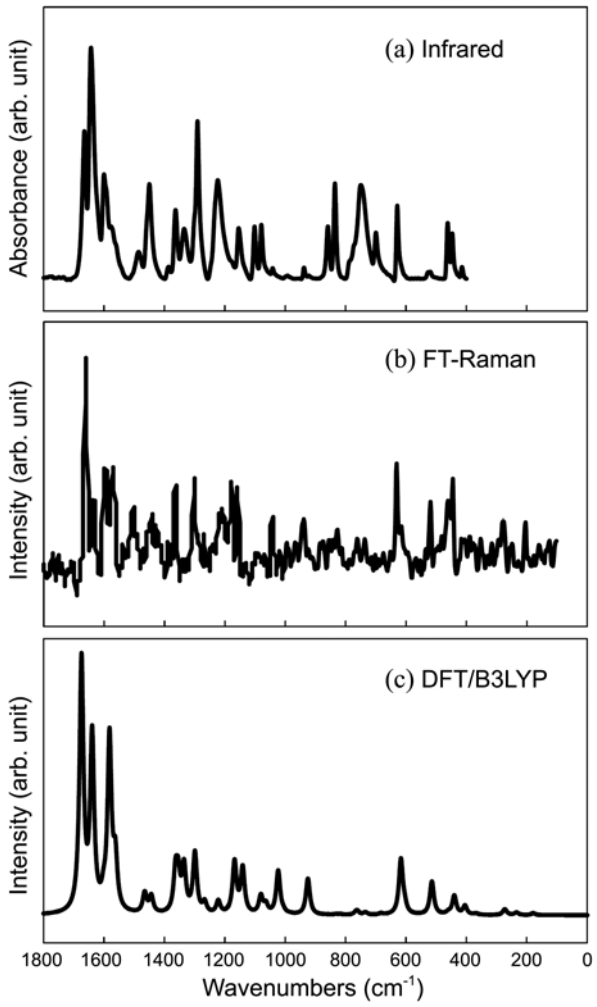

Figure 2. (a) Infrared, (b) powder FT-Raman, and (c) simulated Raman spectra from B3LYP frequencies of juglone. Notice the correlation between the observed and calculated Raman spectra of juglone ((b) and (c)).

The simulated Raman spectrum (Figure 2(c)) is generated from the scaled B3LYP frequencies and Raman activities with 8 cm^{-1} bandwidth. The high intensities of the double-bond stretching bands and the relatively lower band intensities in the finger print region (1500-400 cm^{-1}) are reasonably well reproduced.[8] The observed and computed frequencies and intensities for juglone are compared in Table 1. The ring breathing band observed at 631 cm^{-1} in the FT-Raman spectrum (629 cm^{-1} in the IR spectrum) also corre-

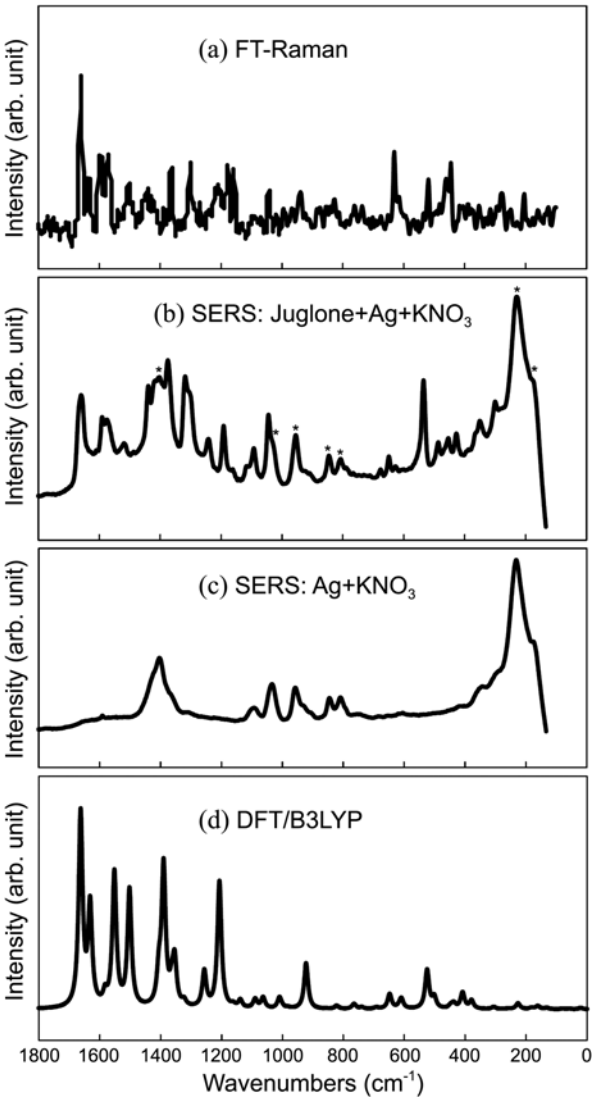

Figure 3. (a) FT-Raman spectrum of juglone powder, SERS spectra of (b) juglone and (c) citrate in Ag colloid, and (d) DFT-computed Raman spectrum of [juglone^{-}···Ag^{+}] complex. In spectrum (b), the peaks denoted with * are due to the citrate anion.

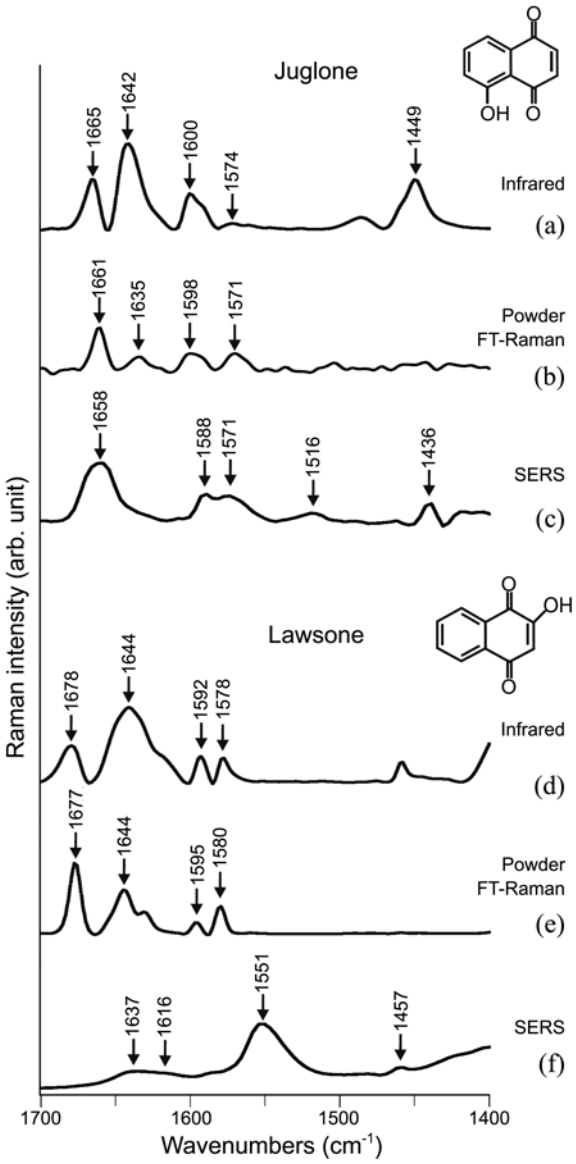

Figure 4. (a) Infrared, (b) power FT-Raman, and (c) SERS spectra in the double-bond stretching region of juglone compared with those of lawsone (d-f). Notice the small red shifts in the SERS spectrum of juglone in contrast to the large shifts in the lawsone spectrum.

lates reasonably well with the scaled B3LYP and BPW 91 frequencies of 617 and 624 cm^{-1}.

The SERS spectrum of juglone is compared with the Ag colloid + KNO_3 spectra and also with the powder FT-Raman spectra in Figure 3, and the measured frequencies from the SERS spectrum are listed in Table 1. While the observed bands are in general weaker than those in the lawsone spectrum,[4] they are still much better resolved than in the previously reported juglone SERS spectrum by Leona *et al*., where many weak bands are barely discernible.[5a] The frequencies of the strong bands generally coincide with the reported values within 5 cm^{-1}, but those of the weaker bands deviate sizably from the previous values.

In the present study, KNO_3 generates the largest surface enhancement for juglone among the aggregating agents used in this study (KNO_3, Na_2SO_4, and $NaOCl_4$).[15] The juglone SERS spectra shown in Figures 3 and 4 are obtained *via* activation with KNO_3. The bands of the citrate anion are sizable, which remains in the sample solution as a remnant of $AgNO_3$ reduction reaction even after washing with distilled water.[15] Addition of NaCl eliminates the juglone bands, indicating substitution of the natural dye adsorbed on the Ag surface by the stronger adsorbent, Cl^{-}.[16]

In Figure 3(b), the strong juglone bands are observed not only in the double-bond stretching but also in the finger print region in the SERS spectrum (also shown in Table 1), whereas in the previously studied lawsone case, the strong bands are observed only in the double-bond stretching and low frequency Ag^{+}···O stretching regions (~400 cm^{-1}). Because only the vibrational motions perpendicular to the Ag surface are supposed to be enhanced by the surface plasmon,[17] the strong SERS bands in the double-bond stretching region

Table 1. Observed and Computed Fundamental Frequencies of Juglone in its Infrared, Powder Raman, and SERS Spectra[a]

Infrared	Powder Raman	Approximate description	B3LYP[b,d]	BPW91[c,d]	SERS	Approximate description	B3LYP[b,e]	BPW91[c,e]
1665 s	1661 vs	C_1-O_{11} str.	1674 (171, 166)	1649 (114, 157)	1658 vs	C_1-O_{11} str. + C_2-C_3 str.	1663 (214)	1642 (238)
1600 s	1598 s	C_2-C_3 str.	1601 (139, 8)	1593 (87, 83)	1588 m	C_2-C_3 str.	1632 (109)	1621 (87)
1574 w	1571 s	C_6-C_7 str.	1562 (54, 31)	1574 (84, 35)	1571 s	C_6-C_7 str.	1583 (12)	1576 (8)
1642 vs	1635 s	C_4-O_{12} str.	1639 (257, 113)	1626 (202, 51)	1516 m	C_4-O_{12} str.	1552 (144)	1533 (196)
	1503 m	Ring A str. + C_4-O_{12} str.	1582 (1, 112)	1562 (23, 103)	1486 w	Ring A str.	1503 (124)	1503 (81)
	1472 w	C_5-O_{13}-H bend + C_9-C_{10} str.	1464 (74, 12)	1470 (147, 17)	1436 m	Ring A str. + C-H bend	1406 (31)	1399 (17)
1449 s	1443 w	Ring A str. + Ring A C-H bend	1443 (77, 10)	1444 (29, 23)	1373 vs	Ring A str. + C-H bend	1390 (145)	1391 (153)
1389 w	1390 w	Ring B str. + Ring B C-H bend	1363 (69, 23)	1377 (57, 18)	1416 w	Ring B str. + C-H bend	1364 (18)	1365 (19)
1333 m	1342 w	C_4-C_{10}-C_5 str.	1335 (87, 27)	1343 (36, 13)	1316 vs	C_4-C_{10}-C_5 str.	1354 (45)	1357 (46)
1302 sh	1301 m	C_5-O_{13} str. + C_4-C_{10} str.	1299 (30, 36)	1303 (33, 37)	1299 s	C_4-C_{10} str.	1323 (6)	1319 (8)
1290 s	1288 w	C_1-C_9 str. + C-H bend	1267 (198, 6)	1276 (196, 16)	1240 m	C_1-C_9 str.	1257 (36)	1258 (68)
1223 s	1221 w	C_4-C_{10}-C_5 str. + C_5-O_{13}-H bend	1221 (122, 7)	1239 (55, 9)	1189 s	C_3-C_4 str. + C_5-C_6 str.	1206 (125)	1215 (96)
1363 s	1364 m	C_9-C_{10} str. + C-H bend	1354 (39, 20)	1387 (45, 36)	1159 w	C_9-C_{10} str. + C-H bend	1162 (3)	1158 (3)
1154 m	1158 m	C-H ip bend + Ring A breath	1141 (36, 26)	1144 (25, 25)	1115 w	Rings A & B C-H bend	1139 (8)	1141 (6)
	1178 m	C-H ip bend	1168 (0, 30)	1168 (0, 29)	1091 m	Ring B C-H bend+ C_7-C_8 str.	1089 (9)	1092 (11)
	1043 m	Ring A breath	1023 (8, 24)	1026 (8, 26)	1042 s	Ring A breathe	1010 (10)	1012 (14)
					954 m	Ring (A & B) deform	922 (42)	925 (30)
					674 w	Ring (A & B) deform	739 (1)	739 (2)
629 s	631 s	Ring breathe (A & B)	617 (23, 28)	624 (20, 40)	647 m	Ring (A & B) breathe	647 (13)	649 (18)
					625 w	C_2-C_1-O_{11} bend	609 (9)	610 (11)
519 w	519 s	Rings A deform	514 (1, 17)	512 (0, 20)	533 vs	Ring A deform	524 (33)	525 (29)
462 m	462 m	C_4-O_{12} bend + C_5-O_{13} bend	460 (11, 1)	463 (11, 1)	485 m	C_4-O_{12} bend + C_5-O_{13} bend	501 (9)	502 (11)
447 m	445 s	Ring B deform	439 (16, 9)	441 (14, 10)	452 m	Ring B deform	437 (4)	439 (4)
414 s	416 w	Ring deform (A & B)	404 (1, 4)	407 (1, 6)				
	353 w	C_{10}-C_5-O bend	368 (10, 1)	373 (9, 1)	347 m	C_{10}-C_5-O_{13} bend	379 (7)	380 (8)
	280 w	C_1-C_9-C_8 bend	273 (1, 3)	277 (1, 4)	297 m	C_1-C_9-C_8 bend	306 (2)	307 (2)

[a]Frequencies and intensities are in cm^{-1} and km/mol. vs, s, m, w, and vw indicate "very strong," "strong," "medium," "weak," and "very weak" [b]Computed with B3LYP/6-311++G(3df,3pd)/SDD (scale factor 0.97). [c]Computed with BPW91/6-311++G(3df,3pd)/SDD. [d]Calculated infrared and Raman intensities in parentheses. [e]Calculated Raman intensities in parentheses.

indicate that the dye molecule is adsorbed perpendicularly to the Ag surface.[4]

The double-bond stretching regions[18] of juglone in the infrared, FT-Raman, and SERS spectra are expanded in Figure 4 for better comparison, and they are also compared with those of lawsone. The relatively small red shifts in the juglone SERS spectrum clearly contrast the large red shifts observed in the lawsone spectra, indicating that weakening of the double-bonds responsible for the observed stretching bands is less significant in coordination of juglone to Ag surface than in the lawsone system.

The strong double-bond stretching bands in the juglone SERS spectrum again suggest that the molecular plane of juglone is perpendicular to the Ag surface. If the molecular plane lies parallel to the Ag surface, the polarizability changes caused by the in-plane double-bond stretching motions would lead to no significant surface plasmonic enhancements. Table 1 and Figure 3 show that the ring-stretching, deformation, and breathing bands are also strong, suggesting that the two rings of juglone are relatively close to the Ag surface so that polarizability changes by these in-plane modes effectively interacts with the surface plasmon.

No C-H out-of-plane bending bands, on the other hand, are observed, which would appear in the region of 1000-650 cm^{-1},[18] while some citrate bands are observed in the region. The absence of these bands is indicative of no enhancement for these bands, consistent with the molecular plane of jugone perpendicular to the Ag surface.

Computations. Juglone, like lawsone,[4] most probably coordinates to the Ag surface *via* its oxygen atom. Juglone is known with its tautomerism and possible release of H^+ as illustrated in Figure 5.[19] Previous reports have suggested that the coordination occurs to an adatom on the Ag surface,

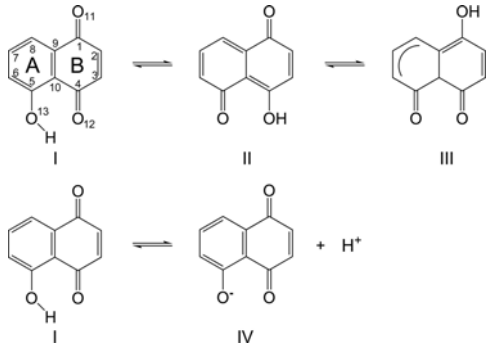

Figure 5. Tautomerism of juglone and release of H^+.

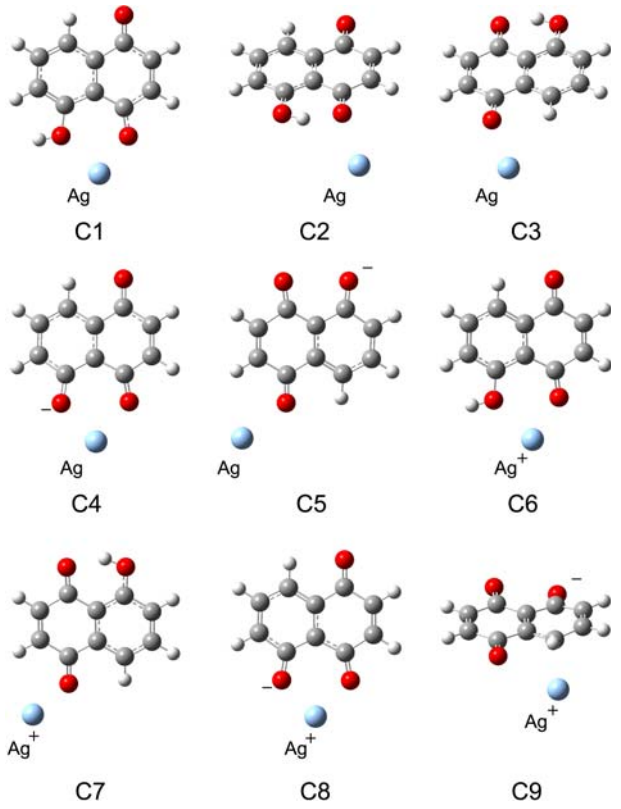

Figure 6. Plausible configurations of juglone (with or without H^+ release) coordinated to an Ag or Ag^+ adatom.

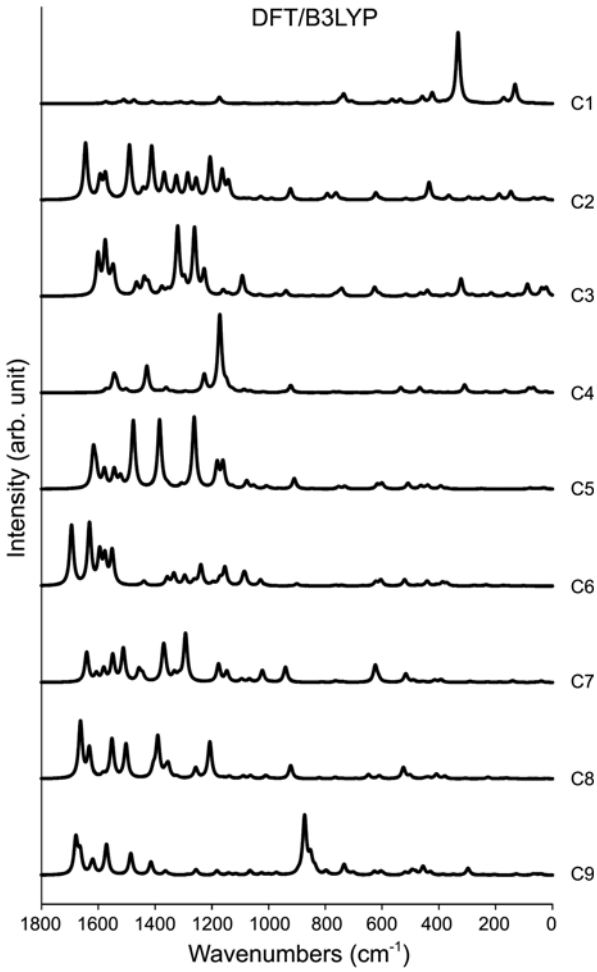

Figure 7. Simulated Raman spectra from the B3LYP frequencies for the configurations of juglone shown in Figure 6.

namely the Ag atom or Ag^+ ion.[20] A recent investigation has also revealed that lawsone coordinated to Ag^+ with H^+ release best reproduces the SERS spectrum.[4] The metal colloid is known to be stabilized by the metal cations adsorbed on the surface of the nono-particles.[21]

DFT computations have been carried out for the tautomeric forms of juglone and coordinated juglone (with and without H^+ release) to an adatom on the Ag surface, and Figure 6 shows the optimized geometries of coordinated juglone (C1-9). Among them, C1-3 show combinations of neutral juglone to an Ag adatom, C4 and 5 combinations of juglone with H^+ release and an Ag adatom, C6 and 7 combinations of neutral juglone to an Ag^+ adatom, and C8 and 9 combinations of juglone with release of H^+ and an Ag^+ adatom. The simulated Raman spectra for these configurations of juglone (with or without H^+ release) coordinated to the Ag or Ag^+ adatom are illustrated in Figure 7. A scale factor of 0.97 is used for the B3LYP frequencies.

In Table 1, the infrared and FT-Raman frequencies correlate reasonably well with the predicted frequencies for tautomer I, which is most stable among the tautomers. Attempts to optimize the geometry of tautomer II end up with that of tautomer I, and tautomer III is 195 kJ/mol higher in energy than tautomer I. The observed bands in the infrared and powder FT-Raman spectra are assigned to the vibrational modes on the basis of their frequencies, relative intensities, and correlation with the DFT results. Unfortunately the isotope substituted products, whose isotopic shifts and intensity variations would further support the assignments, were not available at the time of this work.

Among the examined configurations (C1-9), C8 best reproduces the observed SERS spectrum (Figure 7), C8 being the parallel configuration as in the lawsone case.[4] The measured SERS frequencies are compared with the calculated frequencies for C8 in Table 1, and the observed SERS spectrum with the simulated spectrum of C8 in Figure 3. Notice that the observed SERS bands all originate from in-plane stretching or bending modes. The predicted small red shifts of the double-bond stretching bands for C8 are consistent with the observed values in the SERS spectrum as shown in Table 1 and Figures 3 and 7, which are in contrast to the large red shifts in the lawsone system.

The observed bands in the double-bond stretching region at 1658, 1588, and 1571 cm^{-1} arise from the vibrational modes involving stretching of the C_1-O_{11}, C_2-C_3, and C_6-C_7 bonds, as shown in Table 1, and the polarizability changes of these vibrational modes coincide each other toward the Ag^+ adatom (perpendicular to the Ag surface). Particularly the highest frequency band at 1658 cm^{-1} stems mostly from stretching of the strong C_1-O_{11} bond. The observed bands in the regions of 1500-1000 cm^{-1} originate from the mixed

vibrational modes of the ring-stretching and in-plane C-H bending motions.[18] The SERS bands at 965 (overlapped with a citrate band) and 533 cm^{-1} are also consistent with the ring deformation bands predicted at 922 and 524 cm^{-1}.

Other configurations for coordinated juglone shown in Figure 6 do not reproduce the observed SERS frequencies as well as C8 (Figure 7). C1 yields too low frequencies and intensities for the double-bond stretching bands. C2 is 61 kJ/mol higher than C1, and its low frequency region substantially deviates from the observed spectrum. Coordination of juglone *via* O_{11} to the adatom (C3, 5, and 7) substantially weakens the C_1-O_{11} and C_2-C_3 bonds, and as a result, these configurations fail to reproduce the observed small red shifts of these bands. In C2, 3, and 9, the adatom is located below the molecular plane, and therefore, enhancement of an in-plane vibrational band is expected to be smaller while that of an out-of-plane C-H bending band strong. C4 leads to too large red shifts and too strong in-plane C-H bending bands, whereas C6 yields too high C_1-O_{11} stretching frequency and the strong bands are concentrated in the double-bond stretching region.

Coordinated juglone to the Ag adatom, particularly the stable configurations (C1 and 4), leads to too large red shifts in the double-bond stretching region. In contrast, juglone coordination with or without H^+ release to the Ag^+ adatom, particularly C8, better matches the observed spectrum as shown in Figure 7. It is also expected that coordination to the Ag^+ adatom *via* hydroxyl oxygen prompts H^+ release. The enhanced ring stretching bands in the region of 1500-1000 cm^{-1} in the juglone SERS spectrum are also consistent with C8, both phenol and quinone rings being close to the adatom.

It is interesting that C8 best reproduces the observed SERS spectrum, similar to the lawsone counterpart in the previous study. In both cases, coordination of the natural dyes (with H^+ release) to the Ag^+ adatom yields major characteristics of the SERS spectra, including the small red shifts of the double-bond stretching bands in the juglone system and the much larger shifts in the lawsone system. In juglone, release of H^+ leaves the negative charge in the phenol ring, and thus, it generates relatively small effects to the C_1-O_{11} and C_2-C_3 bonds in the quinone ring. However, in lawsone the negative charge left in the quinone ring is expected to effectively weaken its C_4-O_{13} and C_2-C_3 bonds in the ring. Therefore, the differences in the extents of red shift in the SERS spectra of these natural dyes are in line with H^+ release in coordination to the Ag^+ adatom.

Structure of Juglone Coordinated to Ag^+. DFT computations reveal that the differences in the SERS spectra of juglone and lawsone largely originate from the location of the hydroxyl group in the isomers. Figure 8 shows the structures of juglone (C8) and lawsone coordinated to an Ag^+ adatom. The computed C_1-O_{11} and C_2-C_3 bond lengths of 1.221 and 1.333 Å for coordinated juglone are smaller than the C_4-O_{13} and C_2-C_3 bond lengths of 1.227 and 1.374 Å for coordinated lawsone. These bond lengths vary only slightly upon coordination to the adatom (cf. 1.217 and 1.336 Å for free juglone), whereas in the lawsone system, the corresponding bond lengths change more significantly on coordination (cf. 1.220 and 1.345 Å for free lawsone).

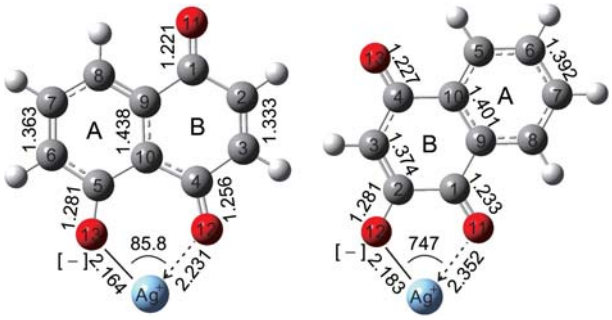

Figure 8. Optimized geometries of (a) juglone and (b) lawsone coordinated to the Ag^+ adatom on Ag surface with H^+ release. DFT computations reveal that the differences in the SERS spectra of juglone and lawsone largely originate from the location of the hydroxyl group in the isomers.

As described above, the double-bond stretching bands arise mostly from the vibrational modes that involve stretching of the C_1-O_{11} and C_2-C_3 bonds (C_4-O_{13} and C_2-C_3 bonds in the lawsone system). The less affected C_1-O_{11} and C_2-C_3 double-bonds in the coordination are consistent with the small frequency shifts in the double-bond stretching region, in contrast to the large red shifts of more than 50 cm^{-1} in the lawsone spectrum.

On the other hand, the C_4-O_{12} bond (1.256 Å) of juglone is much longer than the C_1-O_{11} bond (1.233 Å) of lawsone. Weakening of the juglone C_4-O_{12} bond is consistent with the resonance structures, which increases the negative charge on O_{12}, which in turn strengthens the $O_{12}\cdots Ag^+$ interaction. In contrast, the C_5-O_{13} bond of juglone shortens from 1.334 to 1.281 Å due to release of H^+ and resulting electron delocalization to the aromatic rings. It is also noticeable that unlike the lawsone system, both the aromatic rings of jugone are equally close to the adatom, compatible with the stronger ring-stretching and deformation bands.

Conclusions

The surface enhanced Raman spectrum of juglone, a well-known natural dye, has been investigated with a recently assembled micro-Raman setup, which considerably differs from that of lawsone, a close isomer of juglone. The double-bond stretching bands show only small red shifts from those observed in the infrared and powder Raman spectra, and the strong bands are observed not only in the double-bond stretching but also in the lower frequency ring-stretching and deformation regions.

In an effort to examine the considerable differences in the SERS spectra of these similar isomers, DFT computations have been carried out for the plausible combinations of juglone with or without H^+ release and the Ag or Ag^+ adatom. Among them, a configuration for juglone with H^+ release coordinated to the Ag^+ adatom best reproduces the observed juglone SERS spectrum. The optimized geometry

reveals that the C_1-O_{11} and C-C double-bond lengths vary only slightly, consistent with the observed small red shifts of the double-bond stretching bands. Both the aromatic rings of juglone are close to the adatom, which most probably allow more plasmonic enhancements of the ring-stretching and deformation bands than in the lawsone case. The strong in-plane vibrational bands and absence of the out-of-plane bands suggest that the molecular plane is perpendicular to the metal plane.

Acknowledgments. This work was partially supported by University of Incheon Research Grant in 2010.

References

1. (a) Parras, D.; Vandenabeele, P.; Sánchez, A.; Montejo, M.; Moens, L.; Ramos, N. *J. Raman Spectrosc*. **2010**, *41*, 68. (b) Casadio, F.; Leona, M.; Lombardi, J. R.; Duyne, R. V. *Acc. Chem. Res*. **2010**, *43*, 782. (c) Scherrer, N. C.; Stefan, Z.; Francoise, D; Annette, F; Renate, K. *Spectrochim. Acta A* **2009**, *73*, 5054. (d) Vandenabeele, R.; Edwards, H. G. M.; Moens, L. *Chem. Rev.* **2007**, *107*, 675.
2. (a) Scherrer, N. C.; Stefan, Z.; Francoise, D.; Annette, F.; Renate, K. *Spectrochim. Acta A* **2009**, *73*, 505. (b) Barber, E. J. W. *Prehistoric Textiles: The Development of Cloth in the Neolithic and Bronze Ages with Special Reference to the Aegean*; Princeton University Press, **1991**, ISBN 069100224x.
3. (a) Porter, M. D.; Lipert, R. J.; Siperko, L. M.; Wang, G.; Narayanan, R. *Chem. Soc. Rev.* **2008**, *37*, 1001. (b) Pastoriza-Santos, I.; Alvarez-Puebla, R. A.; Liz-Marzán, L. M. *Eur. J. Inorg. Chem*. **2010**, 4288.
4. Heo, J.-Y.; Cho, C.-H.; Jeon, H.-S.; Cheong, B.-S.; Cho, H.-G. *Spectrochim. Acta A* **2011**, *83*, 425.
5. (a) Leona, M.; Stenger, J.; Ferloni, E. *J. Raman Spectrosc*. **2006**, *37*, 981. (b) Bowie, J. H.; Cameron, D. W.; Williams, D. H. *J. Am. Chem. Soc*. **1965**, *87*, 5094. (c) Lee, A. S.; Mahon, P. J.; Creagh, D. C. *Vib. Spectrosc*. **2006**, *41*, 170. (d) Whitney, A. V.; Van Duyne, R. P.; Casadio, F. *J. Raman Spectrosc*. **2006**, *37*, 993. (e) Pawar, A. B.; Jadhav, K. D.; Gonewar, N. R.; Sarawadekar, R. G. *J. Pharm. Res*. **2011**, *4*, 2051.
6. Hendra, P. J. *Spectrochim. Acta A* **1995**, *51*, 2205.
7. (a) Lee, P. C.; Meisel, D. *J. Phys. Chem*. **1982**, *86*, 3391. (b) Canamares, M. V.; Garcia-Ramos, J. V.; Gomes-Varga, J. D.; Domingo, C.; Sanchez-Cortes, S. *Langmuir* **2005**, *21*, 8546.
8. (a) Jin, R. *J. Mol. Struct*. (*Theochem*) **2010**, *939*, 9. (b) Takasuka, M.; Matsui, Y. *J. C. S. Perkin II* **1979**, 1743. (c) Galasso, V. *Chem. Phys*. **2010**, *374*, 138.
9. Frisch, M. J.; Trucks, G. W.; Schlegel, H. B.; Scuseria, G. E.; Robb, M. A.; Cheeseman, J. R.; Scalmani, G.; Barone, V.; Mennucci, B.; Petersson, G. A.; *et al*. *Gaussian 09*, Revision A.02, Gaussian, Inc.: Wallingford, CT, 2009.
10. (a) Becke, A. D. *J. Chem. Phys.* **1993**, *98*, 5648. (b) Lee, C.; Yang, Y.; Parr, R. G. *Phys. Rev. B* **1988**, *37*, 785.
11. Raghavachari, K.; Trucks, G. W. *J. Chem. Phys*. **1989**, *91*, 1062.
12. Andrae, D.; Haeussermann, U.; Dolg, M.; Stoll, H.; Preuss, H. *Theor. Chim. Acta* **1990**, *77*, 123.
13. (a) Becke, A. D. *Phys. Rev. A* **1988**, *38*, 3098. (b) Burke, K.; Perdew, J. P.; Wang, Y. In *Electronic Density Functional Theory: Recent Progress and New Directions*; Dobson, J. F., Vignale, G., Das, M. P., Ed.; Plenum, 1998.
14. (a) Scott, A. P.; Radom, L. *J. Phys. Chem.* **1996**, *100*, 16502. (b) Andersson, M. P.; Uvdal, P. L. *J. Phys. Chem. A* **2005**, *109*, 2937.
15. Simon, O.; Bumm, L. A.; Callaghan, R.; Blatchford, C. G.; Kerker, M. *J. Phys. Chem*. **1983**, *87*, 1014.
16. Bell, S. E. J.; Sirimuthu, N. M. S. *J. Phys. Chem. A* **2005**, *109*, 7405.
17. Moskovits, M.; Suh, J. S. *J. Phys. Chem*. **1984**, *88*, 5526.
18. Pavia, D. L.; Lampman, G. M.; George, S. K. *Introduction to Spectroscopy*, 3rd Ed.; Brooks Cole: New York, 2000.
19. (a) Thomson, R. H. *Q. Rev. Chem. Soc*. **1956**, *10*, 27. (b) Vessally, E.; Fereyduni, E.; Kamaee, M.; Moradi, S. *J. Serb. Chem. Soc*. **2011**, *76*, 879.
20. (a) Muniz-Miranda, M.; Pergolese, B.; Bigotto, A. *Vib. Spectrosc*. **2007**, *43*, 97. (b) Perry, D. A.; Cordova, J. S.; Spencer, W. D.; Smith, L. G. *J. Phys. Chem. C* **2010**, *114*, 14953. (c) Cardini, G.; Munitz-Miranda, M. *J. Phys. Chem. B* **2002**, *106*, 6875. (d) Pagliai, M.; Bellucci, L.; Munitz-Miranda, M.; Cardini, G.; Schettino, V. *Phys. Chem. Chem. Phys*. **2006**, *8*, 171. (e) Zhao, L.; Jensen, L.; Schatz, G. C. *J. Am. Chem. Soc*. **2006**, *128*, 2911.
21. Sharma, V.; Park, K.; Srinivasara, M. *Mat. Sci. Eng. R*. **2009**, *65*, 1-38 and references therein.